Journal of Photochemistry & Photobiology A: Chemistry 369 (2019) 181–188

Contents lists available at ScienceDirect

Journal of Photochemistry & Photobiology A: Chemistry

journal homepage: www.elsevier.com/locate/jphotochem

$SrSnO_3$ perovskite obtained by the modified Pechini method—Insights about its photocatalytic activity

Ana Rita Ferreira Alves Teixeira[a], Alex de Meireles Neris[a], Elson Longo[c], José Rodrigues de Carvalho Filho[a], Amer Hakki[b], Donald Macphee[b], Ieda Maria Garcia dos Santos[a,b,*]

[a] NPE/LACOM, Núcleo de Pesquisa e Extensão - Laboratório de Combustíveis e Materiais, Universidade Federal da Paraíba, João Pessoa, PB, Brazil
[b] Department of Chemistry, University of Aberdeen, Meston Building, Meston Walk, Aberdeen, UK
[c] CDMF/LIEC, Universidade Estadual Paulista, IQ-UNESP, Araraquara, SP, Brazil

ARTICLE INFO

Keywords:
Photocatalysis
Strontium stannate
Scavenger
Isopropanol
Hydroxyl radical

ABSTRACT

The use of $SrSnO_3$ as a photocatalyst in different applications has been growing in recent years, particularly for degradation of organic dyes. In the present work, $SrSnO_3$ catalyst was synthesized by the modified Pechini method and applied in the photocatalytic degradation of a textile azo-dye in aqueous solution under ultraviolet irradiation. The dominant photocatalytic species for this system were evaluated, determined from terephthalic acid photohydroxylation and from different scavengers. Moreover, electrochemical data were used to evaluate charge transfer between $SrSnO_3$ and the species involved in the photocatalysis – O_2, H_2O and the scavengers. The irradiation time required to achieve 98% decolorization of a Remazol Golden Yellow (RNL) solution was 10 h. The catalyst simultaneously reduced all the absorption bands in the UV–vis spectrum of RNL, suggesting pollutant degradation. Isopropanol, silver and formic acid were all employed to test the importance of different photocatalytic processes and the photohydroxylation of terephthalic acid confirmed the generation of $^{\cdot}OH$. A comparison of the $SrSnO_3$ band positions and the potential of relevant redox couples suggests possible mechanisms for $^{\cdot}OH$ generation from both photogenerated carrier types (electrons and holes), in agreement with the results obtained using the hole/electron scavengers.

1. Introduction

Illumination of a semiconductor photocatalyst with electromagnetic radiation of energy greater than the band gap causes charge separation leading to electron-hole pairs. When recombination does not occur, the separated charge carriers can participate in surface reactions, e.g. oxygen may react with electrons to form the anionic superoxide radical, while water or hydroxide ions may be oxidized by the photogenerated holes. All of these reactions lead to the formation of hydroxyl radicals, which are highly reactive and can degrade organic molecules, such as textile dyes [1].

Among many catalysts employed in photocatalysis, different oxides have recently shown promising results, such as ZnO [2], TiO_2 [3], $CaWO_4$ [4] and others. Oxides with ABO_3 perovskite structure have been highlighted in different photocatalytic reactions but more detailed study on the photocatalytic properties of these materials is still required. For instance, $BiFeO_3$ obtained by solid state reaction and Pechini methods has been applied for tartrazine dye degradation and is considered a promising material for advanced oxidation processes [5]; $BiFeO_3$ based materials have also been employed for photodegradation of methylene blue and rhodamine B dyes [6]. Among stannates, $CaSnO_3$ has been employed in hydrogen evolution from water/ethanol [7], $BaSnO_3$ has been applied to dye solution decolorization [8], and $Ba_{1-x}Sr_xSnO_3$ has been evaluated for water splitting [9]. In studies of photocatalytic hydrogen evolution from pure water, $SrSnO_3$ obtained by solid state reaction [10] and by the wet chemical route [11] showed a high photocatalytic activity. Rod-like $SrSnO_3$ was synthesized by Junploy et al. by cyclic microwave irradiation of a solution containing Sn (II) and Sr(II), followed by calcination to produce the perovskite. The product was used in the methylene blue degradation with 85% of decolorization efficiency [12]. Alammar et al [13] synthesized $SrSnO_3$ by microwave-assisted synthesis in ionic liquids for the photocatalytic H_2 generation. The best results were associated with the large surface area and appropriate band structure of the materials. These authors also

* Corresponding author at: NPE/LACOM, Núcleo de Pesquisa e Extensão - Laboratório de Combustíveis e Materiais, Universidade Federal da Paraíba, João Pessoa, PB, Brazil.
E-mail address: ieda@quimica.ufpb.br (I.M.G. dos Santos).

https://doi.org/10.1016/j.jphotochem.2018.10.028
Received 10 August 2018; Received in revised form 27 September 2018; Accepted 13 October 2018
Available online 15 October 2018
1010-6030/

synthesized $Sr_{1-x}Ba_xSnO_3$ by the same method and observed a higher activity for the $Sr_{0.8}Ba_{0.2}SnO_3$ sample in the hydroxylation of terephthalic acid[14]. In a comparative work involving water splitting with co-catalysts, $CaSnO_3$, $BaSnO_3$ and $SrSnO_3$ were evaluated, and high activities were obtained for $CaSnO_3$ and $SrSnO_3$, when loaded with RuO_2 [15]. For the $ASnO_3$ perovskite, a decrease of the A site cation size leads to an increase of the octahedral tilting and, as a consequence, to the elevation of the conduction band edge potential and a decrease in the potential of the valence band edge which increases the band gap [15,16]. In addition, these distortions influence the band widths which has an impact on the mobility of carriers [15,16].

Although photocatalysis has been reported since the 1960s [17], with well-known applications for environmental remediation [2,18] and alternative sources of energy [3,18], there are still many reasons to study and elucidate the reaction mechanisms of this process, especially for $ASnO_3$ perovskites, which was first applied as photocatalyst at 2006 [10]. Radical reactions and direct oxidation/reduction by holes and electrons are important processes in the degradation of pollutants [2], but whether a direct or an indirect mechanism, i.e., via hydroxyl radicals, plays a major role depends on the reaction conditions and the pollutant to be degraded [19]. Once the major mechanism is known, specific materials can be designed [1,20], the reaction conditions can be improved [20,21] and interfering species can be eliminated [22,23].

Determination of the active species is a crucial aspect of elucidating the reaction pathway [19]. For this purpose, scavengers have been employed to evaluate the participation of each species in photocatalysis [24]. Isopropanol has been employed as a hydroxyl radical scavenger in studies involving the degradation of medical waste [24], herbicides [25], and dyes [26–28]. The alcohol reacts with $^{\cdot}OH$ and generates a more stable tertiary radical, preventing radical oxidation of the dye. Though short aliphatic alcohols also react with holes, according to different authors, direct oxidation is negligible [26,29]. For instance, Chen et al. [26] used methanol and isopropanol to evaluate the role of hydroxyl radicals in the photodegradation of acid orange 7 by TiO_2 and observed that $^{\cdot}OH$ played a minor role in the photoreaction, while iodide was used to scavenge photogenerated holes, and confirmed its important role in the reaction.

Silver ions have been used as electron scavengers during the photocatalytic degradation of phenol [30] and naphthol [31]. Silver nitrate is usually used as the Ag^+ precursor due to its high solubility. Although nitrate ions might generate hydroxyl radicals under UVA light (λ = 365 nm) as described in Eqs. (1) and (2) [32], it has been reported that such effect is less important than the inhibition effect resulting from the UV screening of the photocatalyst [33]. For instance, nitrate ions did not impair the photocatalytic oxidation of rhodamine B in a study that evaluated the influence of inorganic anions on the photocatalytic process [28]. In this sense, the use of the nitrate salt of Ag^+ as an electron scavenger did not trigger any additional effects on the photodegradation reaction.

$$NO_3^- + h\nu \rightarrow NO_3^{\cdot} \rightarrow NO_2 + O^{\cdot} \quad (1)$$

$$O^{\cdot} + H_2O \rightarrow {}^{\cdot}OH + OH^- \quad (2)$$

Formic acid has been employed as hole scavenger in the photocatalytic degradation of nitrates [34], drugs [29] and organic molecules [35,36]. It has also been reported that formic acid can react with holes or hydroxyl radicals, by a direct or indirect mechanism, respectively, as displayed in Eqs. (3) to (6) [37]. According to Salvador et al.[38], the photooxidation mechanism of water dissolved pollutants is directly related to the molecule adsorption onto the photocatalyst surface. When strong adsorption takes place, if it is energetically feasible and with enough illumination flux, an electron may be transferred from the molecule to the semiconductor valence band and direct photooxidation takes place. Formic acid molecules may also react with $^{\cdot}OH$ by an indirect mechanism. For instance, while methanol has weak adsorption onto TiO_2 and is photooxidized by an indirect mechanism, formic acid is more strongly adsorbed on TiO_2 [39,40], which leads to a direct oxidation mechanism, by the photo-Kolbe reaction [41].

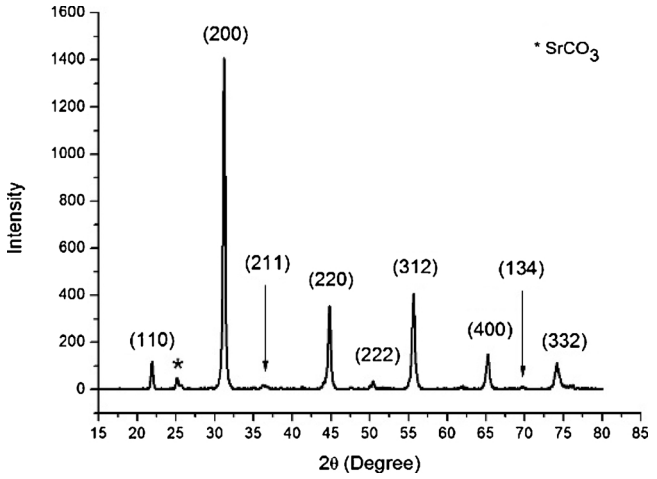

Fig. 1. XRD pattern of the $SrSnO_3$ calcined at 973 K.
Bands assigned to $SrCO_3$ were also observed both in the Raman spectrum (148, 181, 700, 1071 and 1121 cm^{-1}) and the infrared (1771, 1460, 1070 and 860 cm^{-1}) spectrum. The use of an organic medium during the synthetic procedure and the high affinity between Sr^{2+} and CO_3^{2-} led to the formation of this secondary phase [48].

Direct:

$$HCOOH_{(ads)} + h^+ \rightarrow HCOO^{\cdot} + H^+ \quad (3)$$

$$HCOO^{\cdot} + h^+ \rightarrow CO_2 + H^+ \quad (4)$$

Indirect:

$$HCOOH_{(ads)} + {}^{\cdot}OH \rightarrow CO_2H + H_2O \quad (5)$$

$$CO_2H + {}^{\cdot}OH \rightarrow CO_2 + H_2O \quad (6)$$

In this sense, this work aimed to evaluate the efficiency of $SrSnO_3$ in the degradation of an azo dye, and scavengers were employed during photocatalysis to bring insights of the reaction pathways, besides evaluation of the band edge potentials.

2. Experimental

2.1. Catalyst synthesis and characterization

The synthesis of strontium stannate by the modified Pechini method has been previously reported in the literature [42] with a heat treatment at 973 K for 4 h. Metallic tin (99.5%), ammonium hydroxide (P.A), strontium nitrate (99.0%), ethylene glycol (P.A.), all from Vetec (Brazil), nitric acid from FMaia (Brazil), and citric acid from Cargill (Brazil) were employed in the synthesis of $SrSnO_3$.

The prepared $SrSnO_3$ was characterized by X-ray diffraction (XRD), infrared spectroscopy (IR), UV–vis spectroscopy, Raman spectroscopy, Scanning Electron Microscopy (SEM), surface area measurements using the BET method and zeta potential analysis. XRD patterns were obtained with an XRD-6000 Shimadzu diffractometer employing Cu K_α radiation (λ = 0.15406 Å), operated at 2 kVA, 30 V, and 30 mA. The analysis was performed with a 2θ range of 10-90°, a step size of 0.02° and a step time of 2°s^{-1}. The UV–vis spectrum was obtained using a UV-2550 Shimadzu spectrophotometer with a spectral range of 190–900 nm in diffuse reflectance mode; the Wood and Tauc [43] method was employed to graphically determine the band gap. The IR spectrum was obtained with an IRPrestige-21 Shimadzu spectrometer by analysis of a pellet with a mass ratio of 1:100 catalyst:potassium bromide (KBr) in transmittance mode with a spectral range between 400 and 2000 cm^{-1}. To obtain Raman spectra, an inVia Renishaw

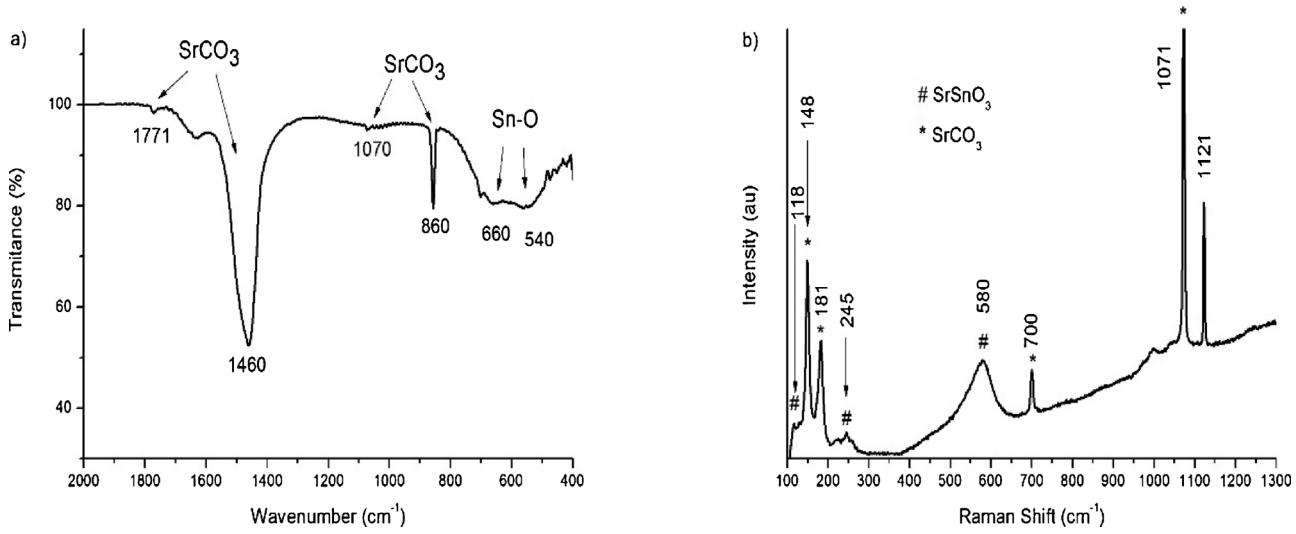

Fig. 2. Infrared (a) and Raman (b) spectra of $SrSnO_3$.

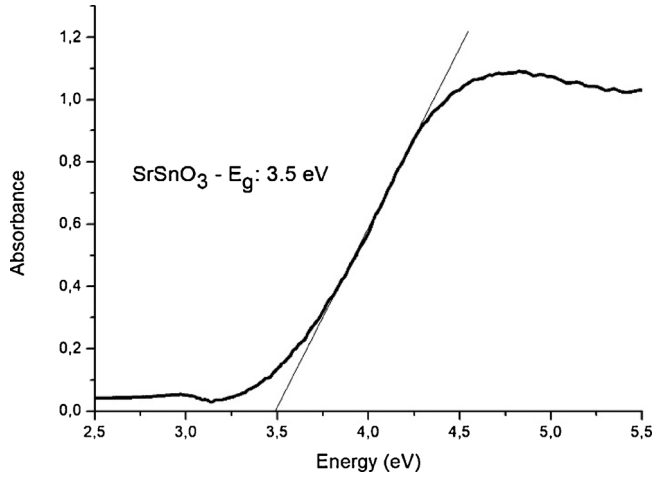

Fig. 3. UV–vis spectrum of $SrSnO_3$.

spectrophotometer was used with a 20 mW Ar laser (518 nm), and the Raman shift was measured in the range between 50 and 1300 cm^{-1}. Scanning electron microscopy (SEM) images were obtained using a Zeiss LEO 1430 equipment.

2.2. Photocatalysis

Photohydroxylation of the terephthalic acid - TA (Alfa aesar) was used as a probe to evaluate the formation of hydroxyl radicals by $SrSnO_3$. This reaction produces 2-hydroxyterephthalic acid, a fluorescent substance [6,14,44]. Briefly, 15.3 mg of $SrSnO_3$ were suspended in 30 mL of the 2 mM NaOH solution containing 0.4 mM of TA, sonicated for 20 min, and illuminated with a 320 nm lamp (0.1 mW cm^{-2}) under magnetic stirring. During the photocatalytic test, aliquots of about 3.0 mL were taken after 1, 2, 3, 4, 6, 8 and 10 h, samples were left under rest in dark conditions overnight and the supernatants were collected and their emission spectra were analyzed in a Hitachi F 2500 fluorescence spectrophotometer, with excitation at $\lambda = 320$ nm; the fluorescence was monitored at $\lambda = 426$ nm, which corresponds to the main fluorescence band of the 2-hydroxyterephthalic acid.

Photocatalytic tests were performed in a magnetic stirred quartz reactor that was irradiated with two 9 W UVC OSRAM Puritec lamps with a main emission at 254 nm A total of 60 mg of catalyst and 90 mL of a 10 $mg.L^{-1}$ of Remazol golden yellow (RNL, from Dystar) aqueous solution were employed in the reaction, with a temperature maintained at 27 °C. Aliquots of the solution were removed with a syringe at different irradiation times and centrifuged for 10 min at 5000 RPM to separate the catalyst. UV–vis spectroscopic analysis of the solution was performed in absorbance mode using the same equipment described above.

Scavengers were used to evaluate the role of the active species in the photodegradation of RNL, and the effect of these scavengers on the process was determined. Isopropanol [24,27] (Moderna, 99.5%), $AgNO_3$ [31] (Cennabras, 99.8%) and formic acid [34] (Panreac, 98%) were employed as hydroxyl radical, electron and hole scavengers, respectively. Based on optimization of the conditions for the use of each scavenger, 0.16 $mol.L^{-1}$ (10,000 times the molar concentration of RNL) isopropanol was employed. The concentration of silver nitrate was 5×10^{-4} $mol.L^{-1}$, as previously reported by Qourzal [31]. The formic acid concentration was limited to 1.6×10^{-3} $mol.L^{-1}$ (100 times the molar concentration of RNL) to avoid a meaningful change in the pH of the RNL solution.

3. Results and discussion

3.1. Catalyst

The XRD pattern of the $SrSnO_3$ catalyst confirmed the crystallization of the orthorhombic structure based on comparison with the ICDD 77–1798 index card; strontium carbonate was identified as a secondary phase (Fig. 1).

The infrared (a) and Raman (b) spectra of the obtained $SrSnO_3$ sample are presented in Fig. 2. Two broad bands are observed in the IR spectra (Fig. 2a) at 540 and 660 cm^{-1}. According to the literature, the bands related to the Sn-O stretching mode of the SnO_3^{2-} groups are located between 500 and 700 cm^{-1} [45,46]. However, according to the profiles of these bands in the present work, a partial short-range disorder is present in this material, whereas $SrSnO_3$ obtained by a solid-state reaction [8] or calcined at a higher temperature presented a narrower band at 670 cm^{-1} [42].

Previous studies of the Raman spectra of orthorhombic stannate perovskites, to which $CaSnO_3$ and $SrSnO_3$ belong, led to the assignment of different frequency ranges in the vibrational spectra. The range below 190 cm^{-1} is associated with lattice soft modes, the range between 190 and 300 cm^{-1} is related to Sn-O bending modes, another range between 300-450 cm^{-1} shows bands assigned to Sn-O_3 torsional modes, and bands related to Sn-O stretching modes are located between 450 and 600 cm^{-1} [15,47,48]. In addition, theoretical studies have

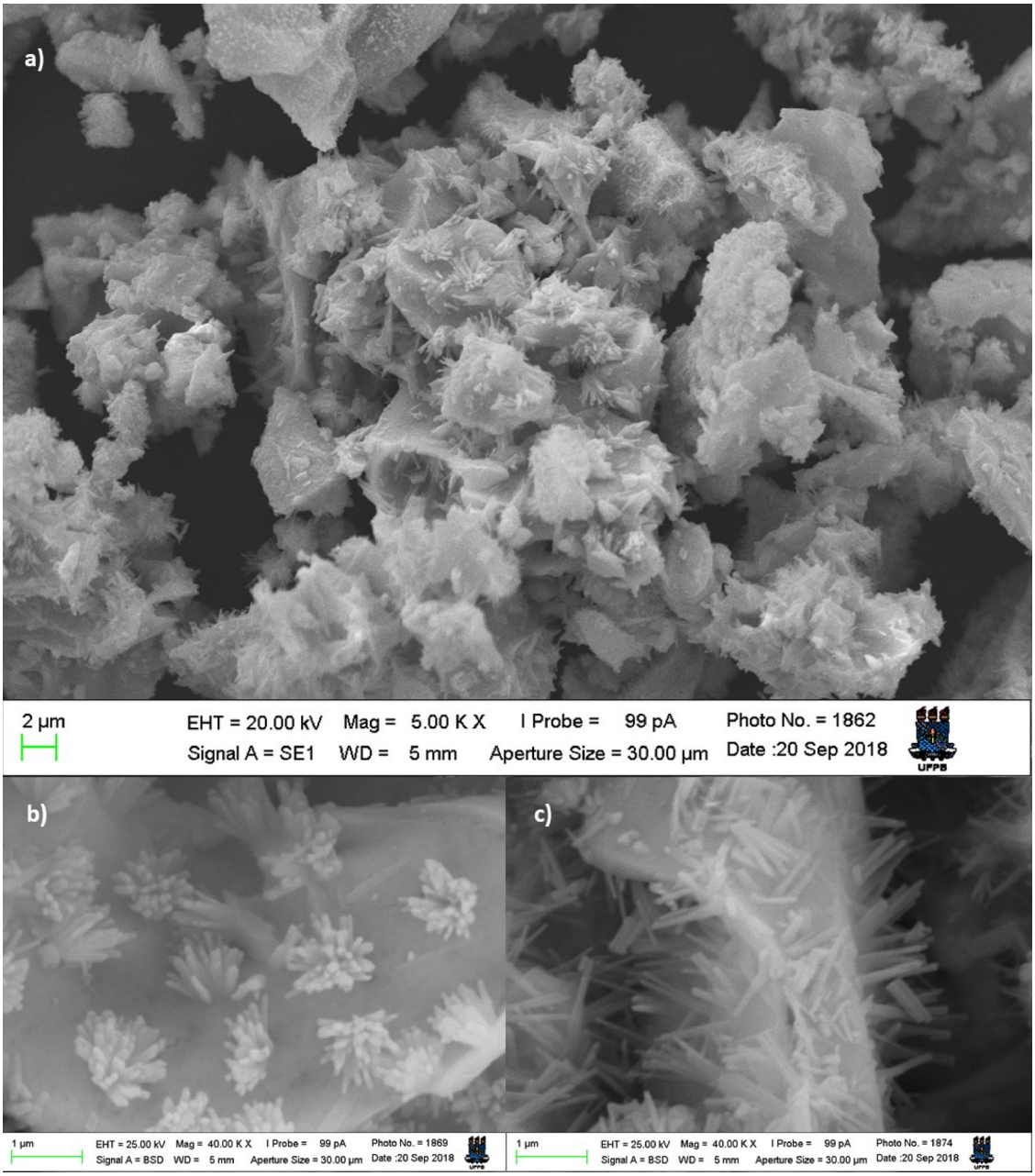

Fig. 4. SEM images of $SrSnO_3$ obtained using secondary electrons (a) and backscattered electrons (b) and (c).

identified bands at approximately 225 cm^{-1}, assigned to scissor movements of the Sn-O-Sn groups along the c axis, and the bands at 252 cm^{-1}, attributed to O-Sn-O bending in the ab plane [46]. In the present work, broad bands were observed at 118 and 245 cm^{-1} in addition to a high intensity, broad band at 580 cm^{-1}. These are usually assigned to defects and may confirm the short-range disorder indicated in the infrared spectrum.

The profile of the UV–vis spectrum (Fig. 3) indicates the short-range disorder in $SrSnO_3$, and a smaller band gap (3.5 eV) compared to that reported for $SrSnO_3$ obtained by different methodologies. For instance, a band gap of 4.0 eV has been reported for strontium stannate obtained by a solid-state reaction [8,15], and a gap of 4.3 eV has been reported for $SrSnO_3$ obtained by the same procedure used in this work but with a calcination temperature of 800 °C, due to a higher short-range order [42].

SEM images of $SrSnO_3$ are displayed in Fig. 4. The material has morphology composed of big agglomerated particles with rods ranging from 450 nm to 2 µm growing from the surface, producing a flower-like morphology (Fig. 4b) or spread over the particles (Fig. 4c). Back-scattered electron imaging indicated the homogeneous distribution of cations throughout the sample.

Despite the higher short-range disorder in the $SrSnO_3$ material prepared by the Pechini method, the lower calcination temperature provided a slightly larger BET surface area (29.1 $m^2.g^{-1}$) than the highest value reported thus far (~27.8 $m^2.g^{-1}$) [11]. This behavior could be related to the needle-like morphology observed by SEM analysis. Concerning the pore size distribution, (BJH method applied to the desorption isotherm), an average pore size of around 4 nm was obtained, although the highest population of pores ranged from 2 to 3 nm (Fig. 5).

As already known concerning metal oxides, at pH values below their pzc, the ionization state of the surface changes according to Eq. (7), while the reaction depicted in Eq. (8) occurs at pH > pzc, changing the ionization state of the surface and its interaction with ionic species

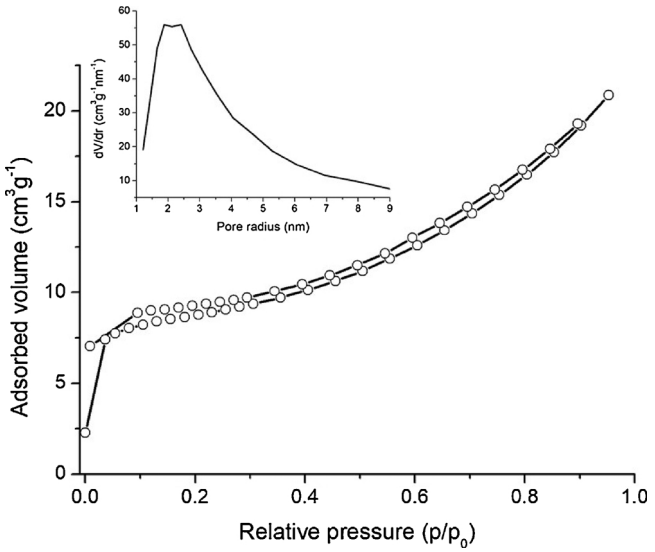

Fig. 5. N_2 adsorption-desorption isotherm for $SrSnO_3$ and BJH pore size distribution (inset).

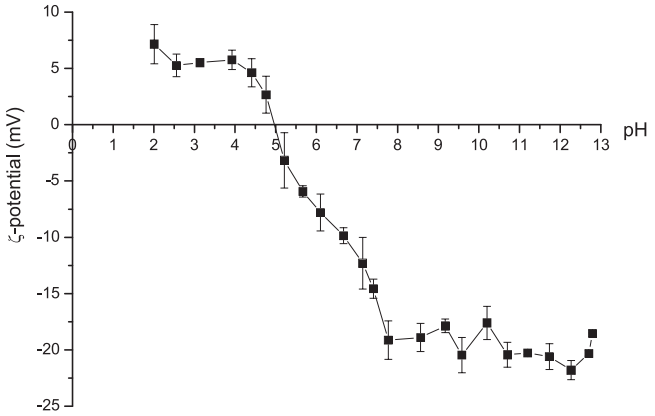

Fig. 6. Zeta potential of $SrSnO_3$ as a function of pH.

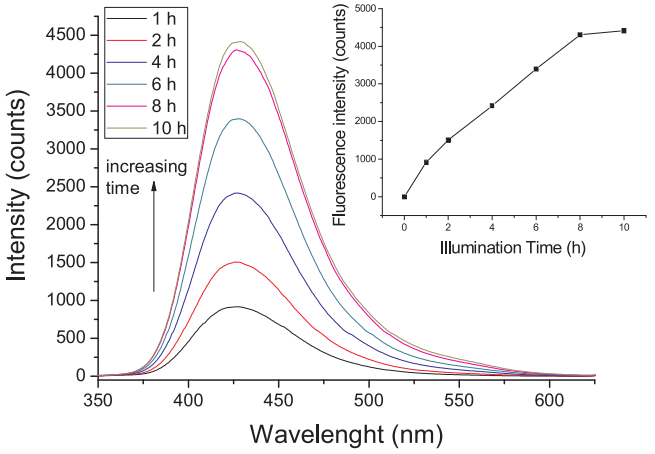

Fig. 7. Fluorescence spectra of the terephthalic acid solution after UVA irradiation in the presence of $SrSnO_3$. Inset: Maximum intensity of the emission band assigned to the 2-hydroxyterephthalic acid, at λ = 426 nm, against the UVA irradiation time.

[49,50]. The pzc value of the obtained $SrSnO_3$ catalyst was found to be at 5 with a meaningful negative variation above this pH, as displayed in Fig. 6.

$$MOH + H^+ \leftrightarrows MOH_2^+ \quad (7)$$

$$MOH + OH^- \leftrightarrows MO^- + H_2O \quad (8)$$

3.2. Photocatalysis

Photohydroxylation of TA over $SrSnO_3$ is presented in Fig. 7. An increase of the absorption intensity at 426 nm is clearly observed up to 8 h, with stabilization after this time, due to the decrease in the amount of TA in solution. Considering the theoretically calculated band edge potentials of the conduction band and of the valence band [51], Alammar [52] proposed that the valence band edge is sufficiently positive for electron donation from water to holes in the valence band, as displayed in Fig. 8, leading to the formation of hydroxyl radicals. However, hydroxyl radical can also be produced following the reaction between adsorbed O_2 and photogenerated electrons in the conduction band, in a two-stage conversion from superoxide ion radical to hydrogen peroxide, as displayed in Eqs. (9) to (11):

$$O_2^{\cdot -} + H^+ \rightarrow HO_2^{\cdot} \quad (9)$$

$$2\ HO_2^{\cdot} \rightarrow H_2O_2 \quad (10)$$

$$H_2O_2 + e^- \rightarrow OH^{\cdot} + OH^- \quad (11)$$

The UV–vis spectrum of the aqueous solution of RNL azo dye shows 3 absorption bands (Fig. 9); one band is related to the azo bond (411 nm), and the other two bands are assigned to the 3-amineacetanilide group (292 and 238 nm) [54]. After 10 h of illumination in the presence of $SrSnO_3$, $SrSnO_3$ was able to decrease the absorption band of the azo bond by 98% and those of the aminoacetanilide group by 94% and 87%, respectively. These results (Fig. 9a) suggest that not only decolorization takes place but also degradation of the RNL molecule occurs in the presence of $SrSnO_3$. Adsorption of RNL onto $SrSnO_3$ was evaluated after 2 h of contact in the dark, but only 2% of decolorization was noticed indicating that this reduction in the concentration is due to photocatalysis rather than only adsorption. As the photocatalytic reaction was performed at pH 6, the material surface is slightly negatively charged according to its determined pzc (see Fig. 6), as well as the ionized RNL (pKa values are 3.0, 3.5 and 6.0 [54]) which decreases the adsorption of the anionic dye because of the repulsing effect. This observation is in agreement with our previous results on $CaSnO_3$ [55] where an adsorption of 8% at pH 6 and 16% at pH 3 was observed. The pzc of $CaSnO_3$ is ~7.3 meaning that the $CaSnO_3$ surface would be positive at these pHs and compatible with the negatively charged dye. However, RNL adsorption on $SrSnO_3$ during photocatalytic testing may not be discarded because of the influence of photogenerated charges [56].

3.2.1. Effects of charge carrier scavengers

Adding isopropanol, as hydroxyl radical scavenger, dramatically inhibited the RNL photocatalysis (Fig. 9b). After 10 h of irradiation in the presence of the scavenger, the absorption bands of the RNL solution with maxima at 411, 292 and 238 nm remained intense, with reductions of only 46%, 27% and 33%, respectively (Fig. 10). These results indicate that an indirect mechanism prevails in the photocatalysis of RNL degradation.

Interestingly, the addition of formic acid (Fig. 9c) has much less effect on the photocatalytic performance than the isopropanol (Fig. 9b) indicating that its presence did not completely prevent the formation of hydroxyl radicals. It is worth mentioning that formic acid addition affected the pH of the RNL solution, causing a decrease in the pH from 5.4 to 3.6. This causes a change of the surface charge from a small negative to a small positive value, which may influence formate adsorption, as already reported for TiO_2 [39], and could also improve the adsorption of the negatively charged RNL dye (pk_{a1} = 3) on the thus positively charged surface [42]. In spite of this, adsorption tests performed in dark

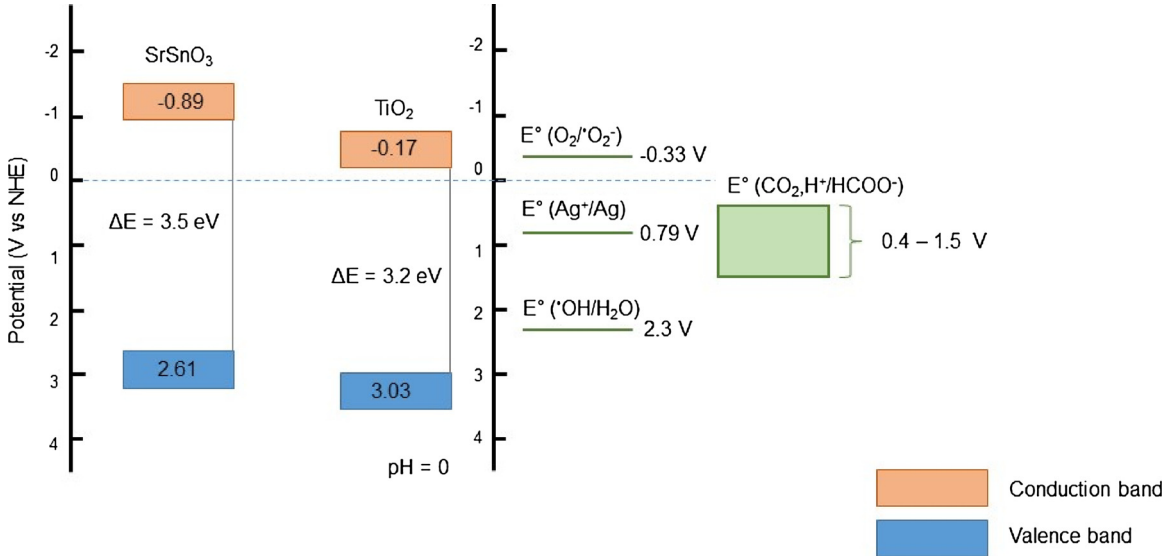

Fig. 8. Energy level diagram illustrating the conduction band (CB) and the valence band (VB) positions of $SrSnO_3$ and TiO_2 with anatase structure, as well as their band gap values. On the right side, standard potential of redox couples involved in the present work are presented for comparison[18]. The oxidation potential for CO_2 formation from formic acid oxidation is show as a range instead of a single value, in agreement to [53].

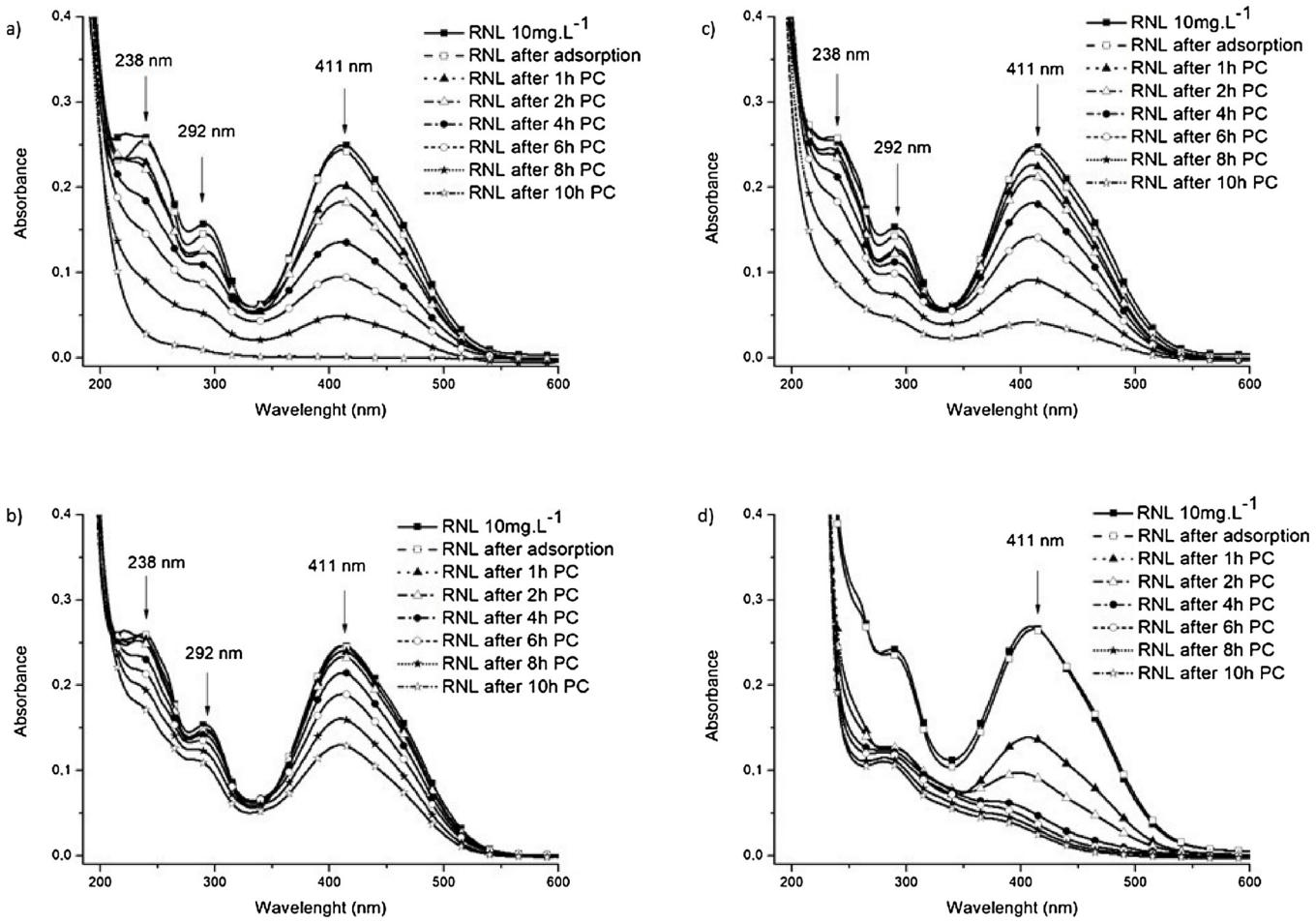

Fig. 9. UV–vis spectra of an RNL solution after different irradiation times. (a) Experiment without additives; (b) experiment employing isopropanol as a hydroxyl radical scavenger; (c) experiment employing formic acid as a hole scavenger; and (d) experiment employing Ag^+ as an electron scavenger.

conditions indicate about 2% of decolorization of the RNL solution after formic acid addition, which may be due to a competition between formate and RNL molecules for the $SrSnO_3$ surface sites, considering also that the molar ratio of formic acid to RNL is 100:1. This competitive adsorption is confirmed by the higher adsorption of RNL at pH 3.6 (6.8% of decolorization), when H_2SO_4 was used to control the pH.

According to Jusys and Behm [53], formic acid oxidation is not as

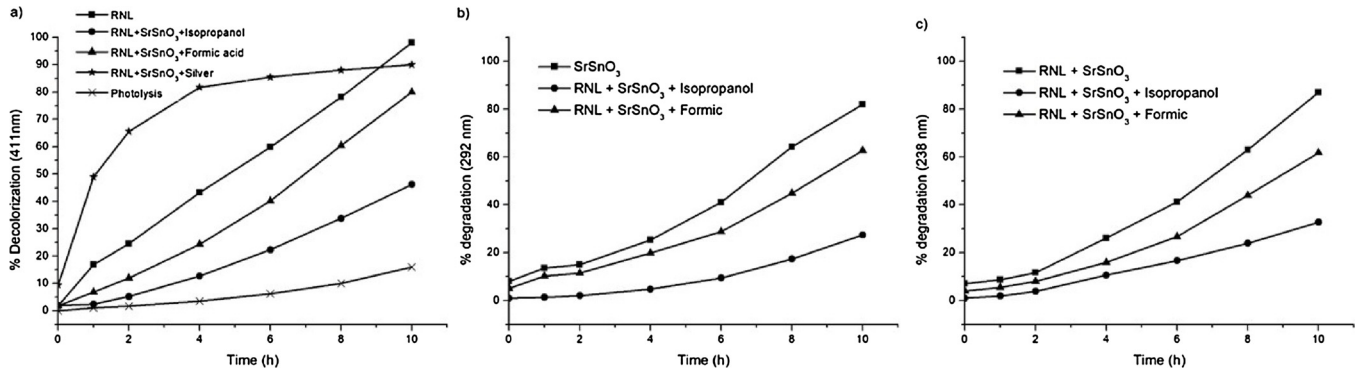

Fig. 10. Decolorization percentages of RNL solutions under different conditions. (a) Absorption band with maximum at 411 nm, assigned to the azo bond; (b) absorption bands with maxima at 292 nm and (c) 238 nm, both assigned to the aminoacetanilide group. Data at time '0' are related to the decolorization due to adsorption after 2 h in the dark, at the same solution conditions.

simple as usually stated in the literature. The authors performed electrochemical experiments using Au film electrodes and measured the oxidation potential for CO_2 formation, whose values varied from 0.4 to 1.5 V, due to the presence of different reaction mechanisms. This range is higher than the valence band edge potential favoring the electron transfer from the formic acid to the valence band of $SrSnO_3$. This behavior is well known for TiO_2 [57,58], which has a valence band edge potential slightly lower than $SrSnO_3$, as displayed in Fig. 8.

Considering information regarding energy and adsorption, in the present case, the decrease of the RNL photodecolorization after formic acid addition indicates that holes have an important role to play in the photocatalytic activity of $SrSnO_3$, by reaction with H_2O and formation of hydroxyl radicals.

On the other hand, when silver ions were added as an electron scavenger, an improvement on the photocatalytic efficiency at the beginning of the reaction was observed (Fig. 9d). Moreover, an increase of the RNL adsorption upon Ag^+ addition into the solution was also observed in dark conditions, with 9.4% of decolorization. After only 1 h of photocatalysis, the absorption bands of the RNL solutions with maxima at 411, 292 and 238 nm were reduced by 49%, 47% and 41%, respectively (Fig. 10). This improvement is even higher after 2 and 4 h of irradiation, but becomes smaller for longer times, with a higher activity for tests done without Ag^+ addition after 10 h of reaction. Upon addition into solution, Ag^+ ions may adsorb on $SrSnO_3$ surface, which should be slightly negatively charged at pH = 6 and electron transfer from the photocatalyst to Ag^+ is energetically favorable (Fig. 8). Moreover, Ag^+ reduction may also occur by photoexcitation. The presence of Ag on the material surface may be responsible for the higher photocatalytic activity, as loaded Ag° provides a Schottky barrier. As a consequence, photogenerated electrons may be transferred from the $SrSnO_3$ conduction band to the Ag, avoiding recombination with photogenerated holes due to this resistive barrier. Ag is also a good site for O_2 adsorption, favoring the superoxide ion radical formation. This behavior was already observed by Junploy et al. [59], who impregnated rod-like $SrSnO_3$ particles with Ag nanoparticles and observed an increase of the photocatalytic decolorization of methylene blue, and by Hu et al. [27], who obtained a higher activity upon adding 2 wt % Ag to a $LaMnO_3$-graphene nanocomposite. Under longer irradiation times, a higher turbidity of the suspension was observed and indicated silver colloid formation, probably due to the high amount of Ag^+ added into the solution. It is likely that the higher suspension turbidity or Ag agglomeration on the photocatalyst surface has inhibited light absorption accounting for the reduced photocatalytic efficiency. The latter mechanism was identified by Junploy et al [59] when the Ag amount increased from 5 to 10 wt %. In the present case, 8.2 wt % of Ag^+ in relation to $SrSnO_3$ was added into the solution.

In addition to decolorization, degradation was also evaluated by the decrease in the intensity of the absorption bands assigned to the aminoacetanilide group (maxima at 292 and 238 nm), as indicated in Fig. 10b and c. A similar behavior was observed after the addition of hydroxyl radical and hole scavengers, further indicating that an indirect mechanism was operative in the photocatalytic reaction. It was not possible to analyze the degradation in the presence of the electron scavenger because the nitrate species absorbed in the same spectral range.

Chládková et al. [60] also evaluated the effect of scavengers on the photocatalytic degradation of an azo dye, Reactive Red 195, in the presence of industrially produced TiO_2 catalysts. Two different catalysts were compared in the work, and different mechanisms seemed to be involved - when PK-180 was employed as the catalyst, hydroxyl radical oxidation was the major route for RR195 degradation. A different behavior was observed by Chen et al. [26] in the photodegradation of Acid Orange 7 by TiO_2 at pH 6. Since the pzc of TiO_2 is 6.8, the catalyst surface was positively charged during photocatalysis, which favors dye adsorption and direct transfer of the hole to the organic molecule. In the photodegradation of Direct Green BE by a Ag-modified $LaMnO_3$-graphene nanocomposite, Hu et al. [27] observed that holes were the most important primary species in the photocatalytic process, whereas hydroxyl radicals played a secondary role.

4. Conclusion

$SrSnO_3$ was successfully synthesized by a modified Pechini method, producing particles with rod-like morphology, a relatively high surface area and a pzc value of 5. The activity of $SrSnO_3$ towards the photocatalytic degradation of the RNL azo-dye was confirmed. Analysis of the energy level diagram of the photocatalyst in comparison with the reacting species was also presented and compared to the results. The use of the scavengers and the use of terephthalic acid as a probe confirmed the important role of the hydroxyl radicals in the photocatalytic degradation of the azo-dye. It was also possible to confirm the role of the holes in the formation of the hydroxyl radicals, by the use of formic acid as a hole scavenger.

Acknowledgements

This work was supported by PROINFRA/FINEP/MCTIC and in part by the Coordenação de Aperfeiçoamento de Pessoal de Nível Superior – Brasil (CAPES) – Finance Code 001.

References

[1] E. Pellizzeti, C. Minero, Mechanism of the photo-oxidative degradation of organic pollutants over TiO_2 particles, Electrochim. Acta 38 (1993) 47–55.
[2] V.S. Kosera, T.M. Cruz, E.S. Chaves, E.R.L. Tiburtius, Triclosan degradation by heterogeneous photocatalysis using ZnO immobilized in biopolymer as catalyst, J. Photochem. Photobiol. A: Chem. 344 (2017) 184–191.

[3] J. Low, B. Cheng, J. Yu, Surface modification and enhanced photocatalytic CO_2 reduction performance of TiO_2: a review, Appl. Surf. Sci. 392 (2017) 658–686.
[4] A. Sahmi, K. Bensadok, M. Trari, Photoelectrochemical properties of $CaWO_4$ synthetized by chemical route. Application to the phenobarbital electro-photocatalysis, J. Photochem. Photobiol. A Chem. 349 (2017) 36–41.
[5] F. Casanova Monteiro, P. de Jesus Cubas, V. Sena Kosera, J.F. Haas Leandro Monteiro, S.T. Fujiwara, Photocatalytic activity of $BiFeO_3$ in pellet form synthetized using solid state reaction and modified Pechini method, J. Photochem. Photobiol. A: Chem. 367 (2018) 390–396.
[6] S. Chaiwichian, K. Wetchakun, W. Kangwansupamonkon, N. Wetchakun, Novel visible-light-driven $BiFeO_3$-Bi_2WO_6 nanocomposites toward degradation of dyes, J. Photochem. Photobiol. A: Chem. 349 (2017) 183–192.
[7] F. Zhong, H. Zhuang, Q. Gu, J. Long, Structural evolution of alkaline earth metal stannates $MSnO_3$ (M = Ca, Sr, and Ba) photocatalysts for hydrogen production, RSC Adv. 6 (2016) 42474–42481.
[8] H.B. Sales, V. Bouquet, S. Députier, S. Ollivier, F. Gouttefangeas, M. Guilloux-Viry, V. Dorcet, I.T. Weber, A.G. De Souza, I.M.G. Dos Santos, $Sr_{1-x}Ba_xSnO_3$ system applied in the photocatalytic discoloration of an azo-dye, Solid State Sci. 28 (2014) 67–73.
[9] Y. Yuan, J. Lv, X. Jiang, Z. Li, T. Yu, Z. Zou, J. Ye, Large impact of strontium substitution on photocatalytic water splitting activity of $BaSnO_3$, Appl. Phys. Lett. 91 (2007) 3–6.
[10] W.F. Zhang, Photoluminescence and photocatalytic properties of $SrSnO_3$ perovskite, Chem. Phys. Lett. 418 (2006) 174–178.
[11] C.W. Lee, D.W. Kim, I.S. Cho, S. Park, S.S. Shin, S.W. Seo, K.S. Hong, Simple synthesis and characterization of $SrSnO_3$ nanoparticles with enhanced photocatalytic activity, Int. J. Hydrogen Energy 37 (2012) 10557–10563.
[12] P. Junploy, S. Thongtem, T. Thongtem, Photoabsorption and photocatalysis of $SrSnO_3$ produced by a cyclic microwave radiation, Superlatt. Microstruct. 57 (2013) 1–10.
[13] T. Alammar, I. Hamm, V. Grasmik, M. Wark, A.-V. Mudring, Microwave-assisted synthesis of perovskite $SrSnO_3$ nanocrystals in ionic liquids for photocatalytic applications, Inorg. Chem. 56 (2017) 6920–6932.
[14] T. Alammar, I.I. Slowing, J. Anderegg, A.-V. Mudring, Ionic-Liquid-Assisted Microwave Synthesis of Solid Solutions of $Sr_{1-x}Ba_xSnO_3$ Perovskite for Photocatalytic Applications, ChemSusChem 10 (2017) 3387–3401.
[15] W. Zhang, J. Tang, J. Ye, Structural, photocatalytic, and photophysical properties of perovskite $MSnO_3$ (M = Ca, Sr, and Ba) photocatalysts, J. Mater. Res. 22 (2007) 1859–1871.
[16] E.H. Mountstevens, S.A.T. Redfern, J.P. Attfield, Order-disorder octahedral tilting transitions in $SrSnO_3$ perovskite, Phys. Rev. B 71 (2005) 2–5.
[17] S.R. Morrison, T. Freund, Chemical Role of Holes and Electrons in ZnO Photocatalysis, J. Chem. Phys. 47 (1543) (1967).
[18] J. Wen, J. Xie, X. Chen, X. Li, A review on g-C_3N_4-based photocatalysts, Appl. Surf. Sci. 391 (2017) 72–123.
[19] C.S. Turchi, Photocatalytic Degradation of Organic Water Contaminants : Mechanisms Involving Hydroxyl Radical Attack, J. Catal. 122 (1990) 178–192.
[20] S.G. Kumar, K.S.R.K. Rao, Comparison of modification strategies towards enhanced charge carrier separation and photocatalytic degradation activity of metal oxide semiconductors (TiO_2, WO_3 and ZnO), Appl. Surf. Sci. 391 (2017) 124–148.
[21] S. Bassaid, D. Robert, M. Chaib, Use of oxalate sacrificial compounds to improve the photocatalytic performance of titanium dioxide, Appl. Catal. B Environ. 86 (2009) 93–97.
[22] M. Mehrvar, Wa. Anderson, M. Moo-Young, Photocatalytic degradation of aqueous organic solvents in the presence of hydroxyl radical scavengers, Int. J. Photoenergy 3 (2001) 187–191.
[23] C. Hu, J.C. Yu, Z. Hao, P.K. Wong, Effects of acidity and inorganic ions on the photocatalytic degradation of different azo dyes, Appl. Catal. B Environ. 46 (2003) 35–47.
[24] R. Palominos, J. Freer, M.A. Mondaca, H.D. Mansilla, Evidence for hole participation during the photocatalytic oxidation of the antibiotic flumequine, J. Photochem. Photobiol. A: Chem. 193 (2008) 139–145.
[25] A. Amine-Khodja, A. Boulkamh, C. Richard, Phototransformation of metobromuron in the presence of TiO_2, Appl. Catal. B Environ. 59 (2005) 147–154.
[26] Y. Chen, S. Yang, K. Wang, L. Lou, Role of primary active species and TiO_2 surface characteristic in UV-illuminated photodegradation of Acid Orange 7, J. Photochem. Photobiol. A: Chem. 172 (2005) 47–54.
[27] J. Hu, J. Men, Y. Liu, H. Huang, T. Jiao, One-pot synthesis of Ag-modified $LaMnO_3$ –graphene hybrid photocatalysts and application in the photocatalytic discoloration of an azo-dye, RSC Adv. 5 (2015) 54028–54036.
[28] C. Yang, J. Yu, Q. Li, Y. Yu, Facile synthesis of monodisperse porous ZnO nanospheres for organic pollutant degradation under simulated sunlight irradiation: The effect of operational parameters, Mater. Res. Bull. 87 (2017) 72–83.
[29] R.P. Cavalcante, R.F. Dantas, B. Bayarri, O. González, J. Giménez, S. Esplugas, A. Machulek, Photocatalytic mechanism of metoprolol oxidation by photocatalysts TiO_2 and TiO_2 doped with 5% B: Primary active species and intermediates, Appl. Catal. B Environ. 194 (2016) 111–122.
[30] Z. Li, J. Sheng, Y. Zhang, X. Li, Y. Xu, Environmental Role of CeO_2 as oxygen promoter in the accelerated photocatalytic degradation of phenol over rutile TiO_2, Appl. Catal. B Environ. 166–167 (2015) 313–319.
[31] S. Qourzal, N. Barka, M. Tamimi, A. Assabbane, Photodegradation of 2-naphthol in water by artificial light illumination using TiO_2 photocatalyst: Identification of intermediates and the reaction pathway, Appl. Catal. A Gen. 334 (2008) 386–393.
[32] M.K. Kim, K.D. Zoh, Effects of natural water constituents on the photo-decomposition of methylmercury and the role of hydroxyl radical, Sci. Total Environ. 449 (2013) 95–101.
[33] M.N. Chong, B. Jin, C.W.K. Chow, C. Saint, Recent developments in photocatalytic water treatment technology: a review, Water Res. 44 (2010) 2997–3027.
[34] S. Rengaraj, X.Z. Li, Enhanced photocatalytic reduction reaction over Bi^{3+}-TiO_2 nanoparticles in presence of formic acid as a hole scavenger, Chemosphere 66 (2007) 930–938.
[35] N. De La Cruz, V. Romero, R.F. Dantas, P. Marco, B. Bayarri, J. Giménez, S. Esplugas, O-Nitrobenzaldehyde actinometry in the presence of suspended TiO_2 for photocatalytic reactors, Catal. Today 209 (2013) 209–214.
[36] S. Zheng, Y. Cai, K.E. O'Shea, TiO_2 photocatalytic degradation of phenylarsonic acid, J. Photochem. Photobiol. A: Chem. 210 (2010) 61–68.
[37] J.M. Kesselman, O. Weres, N.S. Lewis, M.R. Hoffmann, Electrochemical Production of Hydroxyl Radical at Polycrystalline Nb-Doped TiO_2 Electrodes and Estimation of the Partitioning between Hydroxyl Radical and Direct Hole Oxidation Pathways, J. Phys. Chem. B 101 (1997) 2637–2643.
[38] D. Monllor-Satoca, R. Gómez, M. González-Hidalgo, P. Salvador, The 'Direct-Indirect' model: An alternative kinetic approach in heterogeneous photocatalysis based on the degree of interaction of dissolved pollutant species with the semiconductor surface, Catal. Today 129 (2007) 247–255.
[39] T. Lana Villarreal, R. Gómez, M. Neumann-Spallart, N. Alonso-Vante, P. Salvador, Semiconductor photooxidation of pollutants dissolved in water: A kinetic model for distinguishing between direct and indirect interfacial hole transfer, J. Phys. Chem. B 108 (2004) 15172–15181.
[40] Y. Nosaka, A.Y. Nosaka, Generation and Detection of Reactive Oxygen Species in Photocatalysis, Chem. Rev. 117 (2017) 11302–11336.
[41] I.K. Konstantinou, T.A. Albanis, TiO_2-assisted photocatalytic degradation of azo dyes in aqueous solution: kinetic and mechanistic investigations: a review, Appl. Catal. B Environ. 49 (2004) 1–14.
[42] G.L. Lucena, J.J.N. Souza, A.S. Maia, L.E.B. Soledade, E. Longo, A.G. Souza, I.M.G. Santos, New methodology for a faster synthesis of $SrSnO_3$ by the modified Pechini method, Cermica 59 (2013) 249–253.
[43] D.L. Wood, J. Tauc, Weak absorption tails in amorphous semiconductors, Phys. Rev. B 5 (1972) 3144–3151.
[44] K. Ishibashi, A. Fujishima, T. Watanabe, K. Hashimoto, Quantum yields of active oxidative species formed on TiO_2 photocatalyst, J. Photochem. Photobiol. A: Chem. 134 (2000) 139–142.
[45] M.C.F. Alves, S.C. Souza, M.R.S. Silva, E.C. Paris, S.J.G. Lima, R.M. Gomes, E. Longo, A.G. De Souza, I.M. Garcia Dos Santos, Thermal analysis applied in the crystallization study of $SrSnO_3$, J. Therm. Anal. Calorim. 97 (2009) 179–183.
[46] E. Moreira, J.M. Henriques, D.L. Azevedo, E.W.S. Caetano, V.N. Freire, E.L. Albuquerque, Structural, optoelectronic, infrared and Raman spectra of orthorhombic $SrSnO_3$ from DFT calculations, J. Solid State Chem. 184 (2011) 921–928.
[47] M. Tarrida, H. Larguem, M. Madon, Structural investigations of (Ca,Sr)ZrO_3 and Ca(Sn,Zr)O_3 perovskite compounds, Phys. Chem. Miner. 36 (2009) 403–413.
[48] M.C.F. Alves, M.R. Nascimento, S.J.G. Lima, P.S. Pizani, J.W.M. Espinosa, E. Longo, L.E.B. Soledade, A.G. Souza, I.M.G. Santos, Influence of synthesis conditions on carbonate entrapment in perovskite $SrSnO_3$, Mater. Lett. 63 (2009) 118–120.
[49] M. Antonopoulou, I. Konstantinou, TiO_2photocatalysis of 2-isopropyl-3-methoxy pyrazine taste and odor compound in aqueous phase: Kinetics, degradation pathways and toxicity evaluation, Catal. Today 240 (2014) 22–29.
[50] U.G. Akpan, B.H. Hameed, Parameters affecting the photocatalytic degradation of dyes using TiO_2-based photocatalysts: a review, J. Hazard. Mater. 170 (2009) 520–529.
[51] M.A. Butler, D.S. Ginley, Prediction of Flatband Potentials at Semiconductor-Electrolyte Interfaces from Atomic Electronegativities, J. Electrochem. Soc. 125 (1978) 228–232.
[52] T. Alammar, I.I. Slowing, J. Anderegg, A.-V. Mudring, Ionic-Liquid-Assisted, ChemSusChem 10 (2017) 3387–3401.
[53] Z. Jusys, R.J. Behm, Electrooxidation of formic acid on a polycrystalline Au film electrode–A comparison with mass transport limited bulk CO oxidation and kinetically limited oxalic acid oxidation, J. Electroanal. Chem. Lausanne (Lausanne) 800 (2017) 60–76.
[54] M. Catanho, G.R.P. Malpass, A. Motheo, J. de, Evaluation of electrochemical and photoelectrochemical methods for the degradation of three textile dyes, Quim. Nova 29 (2006) 983–989.
[55] G.L. Lucena, L.C. De Lima, L.M.C. Honório, A.L.M. De Oliveira, R.L. Tranquilim, E. Longo, A.G. De Souza, A. Da S Maia, I.M.G. dos Santos, $CaSnO_3$ obtained by modified Pechini method applied in the photocatalytic degradation of an azo dye, Ceramica 63 (2017) 536–541.
[56] P. Borthakur, P.K. Boruaha, N. Hussaina, Y. Silla, M.R. Das, Specific ion effect on the surface properties of Ag/reduced graphene oxide nanocomposite and its influence on photocatalytic efficiency towards azo dye degradation, Appl. Surf. Sci. 423 (2017) 752–761.
[57] T.T.Y. Tan, D. Beydoun, R. Amal, Photocatalytic reduction of Se(VI) in aqueous solutions in UV/TiO_2 system: Importance of optimum ratio of reactants on TiO_2 surface, J. Mol. Catal. A Chem. 202 (2003) 73–85.
[58] V.N.H. Nguyen, D. Beydoun, R. Amal, Photocatalytic reduction of selenite and selenate using TiO_2 photocatalyst, J. Photochem. Photobiol. A: Chem. 171 (2005) 113–120.
[59] P. Junploy, T. Thongtem, S. Thongtem, A. Phuruangrat, Decolorization of Methylene Blue by Ag/$SrSnO_3$ Composites under Ultraviolet Radiation, J. Nanomater. 2014 (2014) 1–10.
[60] B. Chládková, E. Evgenidou, L. Kvítek, A. Panáček, R. Zbořil, P. Kovář, D. Lambropoulou, Adsorption and photocatalysis of nanocrystalline TiO_2 particles for Reactive Red 195 removal: effect of humic acids, anions and scavengers, Environ. Sci. Pollut. Res. 22 (2015) 16514–16524.